Journal of Non-Crystalline Solids 476 (2017) 60–66

Contents lists available at ScienceDirect

Journal of Non-Crystalline Solids

journal homepage: www.elsevier.com/locate/jnoncrysol

Viscous flow flash sintering of porous silica glass

Miguel Oscar Prado[a,b], Mattia Biesuz[c,d,*], Matteo Frasnelli[c], Franco Emmanuel Benedetto[a], Vincenzo M. Sglavo[c,d]

[a] Departamento Materiales Nucleares, Centro Atómico Bariloche, Comisión Nacional de Energía Atómica, Km.9.5Av E. Bustillo, 8400 San Carlos de Bariloche, Argentina
[b] Consejo Nacional de Investigaciones Científicas y Técnicas (CONICET), 8400 San Carlos de Bariloche, Argentina
[c] Department of Industrial Engineering, University of Trento, Via Sommarive 9, 38123 Trento, Italy
[d] INSTM Research Unit, Via G. Giusti 9, 50121 Firenze, Italy

ARTICLE INFO

Keywords:
Sintering
Silicate glass
Flash sintering
Electric field induced softening
Powder
Consolidation

ABSTRACT

For the first-time compacts of porous glass particles (95 wt% SiO_2, 2.3% Na_2O, 1.6% Al_2O_3) exhibiting macro-, meso- and micro-pores were densified by flash sintering, using DC electric field in the range 1000–3000 V cm^{-1}. The results point out the applicability of this sintering technology to glasses characterized by viscous flow sintering mechanisms. Excluding the anodic region, the specimens resulted well densified using a current limit of 2 mA mm^{-2} and a dwelling time of 30 s. The obtained microstructure at the anode and at the cathode side is asymmetric, the former being characterized by the formation of Na-enriched region, the latter by the local formation of large pores (hundreds of microns). The mechanism, which triggers the flash event, appears to be associated to dielectric breakdown.

1. Introduction

Flash Sintering (FS) is an innovative, electric field-assisted sintering technique which allows a consistent reduction of consolidation time and temperature for crystalline ceramics [1–11]. Indeed, the densification takes place in few seconds at an onset furnace temperature, strictly related to the applied field [12,13], much lower than that needed in the conventional processes.

In a typical flash sintering experiment, a constant electrical field is applied to a green ceramic specimen subjected to isothermal or constant heating rate treatment. Since ceramic materials are characterized by negative temperature coefficient for electrical resistivity, the current flowing through the material gradually increases during the flash sintering experiments. Once an opportune combination of field and temperature is reached, an abrupt drop of the electrical resistivity is observed [1,2,14,15] and a rapid densification takes place, accompanied by some unusual effects like a very strong photoemission [16–18]. The combination of these phenomena is at the base of the so-called flash event. The current flowing through the material is usually limited to avoid damages by setting a current limit in the power source. Once the flash event occurs, the power supply reaches such current limit and then the electric current is kept constant for a certain time.

In 2015, McLaren et al. have shown that also amorphous materials can reproduce a sort of flash event. This has been detected in alkali-containing silicate glass samples [19] where a viscosity reduction was observed at given combination of electric field and furnace temperature, the phenomenon being therefore named as Electric Field-Induced Softening (EFIS).

Recently, flash sintering was applied to an intermediate system containing both crystalline (alumina) and amorphous phase (magnesia-silicate glass) [20]. The current flow was shown to allow rapid densification via liquid phase sintering mechanisms at unusually low temperatures. Conversely, when silica glass-containing alumina system was considered, flash event could not be reproduced [20]. As a matter of fact, according to previous findings [21], very resistive materials cannot be flash sintered, the high electrical resistivity of pure silica inhibiting the runaway for the flash event.

The idea arose to apply the flash sintering process to amorphous materials where the viscous flow activation observed by McLaren et al. on bulk glass specimens could trigger the densification phenomena in glass powder compact. The aim of the present work is therefore to show whether electric field-induced softening could be used for reducing the consolidation time and temperature of amorphous materials, namely nearly-pure porous silica glass.

2. Materials, methods and calculations

2.1. Glass preparation and characterization

Sodium borosilicate glass with composition (wt%) 65.6 SiO_2 – 27.8

* Corresponding author at: Department of Industrial Engineering, University of Trento, Via Sommarive 9, 38123 Trento, Italy.
E-mail address: mattia.biesuz@unitn.it (M. Biesuz).

http://dx.doi.org/10.1016/j.jnoncrysol.2017.09.024
Received 17 July 2017; Received in revised form 21 August 2017; Accepted 5 September 2017
Available online 21 September 2017

B_2O_3 – 6.0 Na_2O - 0.6 Al_2O_3, was produced in the present work by using the following reagents: silicon dioxide - SiO_2 (Fluka Analytical, 99.87%), sodium tetraborate - $B_4Na_2O_7{\cdot}10\ H_2O$ (Sigma-Aldrich, 99.5%), boron trioxide - B_2O_3 (Riedel-De Haën, 99.94%) and Aluminum oxide - Al_2O_3 (Sigma-Aldrich, 99.7%). After drying the reagents at 115 °C, they were mixed and left to homogenize under mechanical stirring for 20 h. Then, the powder mixture was put into a high purity platinum crucible and heated up to 1600 °C for 2 h in a Deltech DT-31 furnace. The molten material was poured onto a thick steel plate and rapidly pressed with another steel plate: this technique, known as splat-cooling, allows high cooling rates of around 200 °C/s. The obtained glass was then treated at 660 °C for 12 h to promote spinodal liquid phase separation. The glass was manually ground in an agate mortar and the powder was treated in distilled water at 90 °C for 24 h to leach away the Na-B rich phase. After two consecutive washing with distilled water and drying at 90 °C micrometric and nanometric porosity was produced.

The particle size distribution was measured using a Malvern Mastersizer particle size analyzer. Moreover, the produced glass was characterized by energy dispersive spectroscopy X-Ray Fluorescence (XRF), using a S8 Tiger(4 kW) spectrometer from Bruker, and by Differential Thermal Analysis (DTA), using a Q600 analyzer from TA Instruments at 10 °C min^{-1}, in order to determine the final chemical composition and the glass transition temperature, respectively.

2.2. Flash sintering and sample characterization

Cylindrical pellets (diameter ≈ 6 mm, thickness ≈ 4 mm) were produced by uniaxial pressing at 150 MPa using distilled water as binder. The samples were then introduced into a specifically modified dilatometer (Linseis L75), where flash sintering experiments were carried out. The samples were placed between two platinum discs (diameter = 9 mm) used as electrodes. These were electrically connected to a DC power supply (Glassman EW series 5 kV–120 mA) and to a multimeter (Keithley 2100). The electrical parameters, as well as sample shrinkage and furnace temperature, were recorded at 1 Hz. The dilatometer piston was set to apply a load of 500 mN (≈ 17.7 kPa) to ensure good contact between electrodes and glass specimen. The experiments were carried out in static air, using constant heating rate of 10 °C min^{-1}. Different electric fields were used from 0 to 3000 V cm^{-1}. The current limit was fixed at 60 mA (2.0 mA mm^{-2}) for most of the experiments. Other current values (5, 15, 100 mA) were also used for comparison during isothermal treatments at 690 °C. In all cases, the current was let to flow for < 2 min after that the current limit was reached; then, the power supply and the furnace were turned off.

The flash sintered specimen density was determined by the Archimedes' method; the possible presence of crystalline phases was checked by X-Ray Diffraction (XRD, Italstrutture CPS) working with Cu-Kα radiation (8.08 keV) at 40 kV and 30 mA in 2θ range of 10–100°. The samples microstructure was analyzed by observing polished surfaces (by using SiC 1200 paper) under SEM (Jeol JSM 5500). EDS analysis (JEOL IXRF SYSTEMS 500, software Iridium Ultra) were carried out at 20 kV on the anodic and cathodic regions and on the starting glass powder.

2.3. Sample temperature calculation

During the flash sintering experiment, the actual sample temperature (T_S) is likewise higher than the measured furnace temperature (T_F) owing to the current flow along the sample. In order to estimate the real sample temperature, one can consider that the sample temperature derivative with respect to time, dT_S/dt (t = time) is proportional to the difference between power input W_{in} and output W_{out}:

$$mC_p\frac{dT_S}{dt} = W_{in} - W_{out} \tag{1}$$

m and C_p (equal to 1.2 J g^{-1} K^{-1}) being the mass and the specific heat.

Eq. (1) is valid under the following assumptions:

i. The sample is heated as a whole: macroscopic (i.e. between the center and the surface or between the two electrodes) and microstructural (i.e. between the particles surface and core) temperature differences are neglected;
ii. No phase transition occurs.

On such bases, Eq. (1) provides an estimation of the average thermal evolution of the system during the flash process and does not pretend to provide the calculation of the exact sample temperature, also considering that strong temperature gradients may be generated during the flash [22–26].

The power input is the energy dissipated by Joule heating (W_{in} = V I); the power output can be identified with the radiation losses through the lateral surface of the sample. Therefore,

$$mC_p\frac{dT_s}{dt} = VI - \sigma\varepsilon S_{lat}(T_s^4 - T_f^4) \tag{2}$$

where σ is the Stefan-Boltzmann constant, ε the sample emissivity (assumed equal to 1) and S_{lat} the lateral surface of the specimen.

For two consecutive times (t_1 and t_2), the sample temperature changes according to:

$$T_{s2} = T_{s1} + \frac{t_2 - t_1}{mC_P}[V_1I_1 - \sigma\varepsilon S_{lat1}(T_{s1}^4 - T_{f1}^4)] \tag{3}$$

Such equation can therefore be used for estimating the sample temperature evolution.

3. Results and discussion

The chemical composition of the glass powder is reported in Table 1. The analysis confirms the efficiency of the production route, the material being essentially constituted by pure silica (95 wt%), alumina (1.6 wt%) and a residual amount of Na_2O, around 2.3 wt%.

The glass transition temperature, Tg, determined from the diagram in Fig. 1(a) is equal to 888 °C. Fig. 1(b) shows the particle size distribution of the silica glass constituted by powders with a size for the 50% accumulated volume D(v,0.5) of 55.7 ± 0.1 μm.

3.1. Flash sintering experiments

Fig. 2 reports the dilatometric curves of the green glass samples measured at constant heating rate (10 °C min^{-1}) varying the applied E-field. Starting from the conventional treatment (0 V cm^{-1}), the glass powder begins to shrink around 600 °C, then the shrinkage proceeds with a moderate rate at higher temperature.

Conversely, if E ≥ 1000 V cm^{-1}, the flash event occurs with an abrupt and instantaneous increase of the sintering rate, consistent with previous findings on crystalline ceramics; as expected, also the onset temperature for the flash event decreases with the applied electric field (inset in Fig. 2) [2,12,14]. It is interesting to observe that under 3000 V cm^{-1} the material is flash sintered at about 600 °C, temperature at which only very preliminary densification mechanisms are activated in conventional processes. We can also observe that the dilatometric plots of the samples treated with or without field are exactly overlapped until the flash event takes place this being particularly evident if samples treated with 0 and 1000 V cm^{-1} are compared. Therefore, the E-

Table 1
Chemical composition (wt%) of the glass powder.

SiO_2	Na_2O	Al_2O_3	P_2O_5	CaO	K_2O	TiO_2	Fe_2O_3	Y_2O_3
95	2.3	1.6	0.60	0.12	0.090	0.032	0.023	0.007

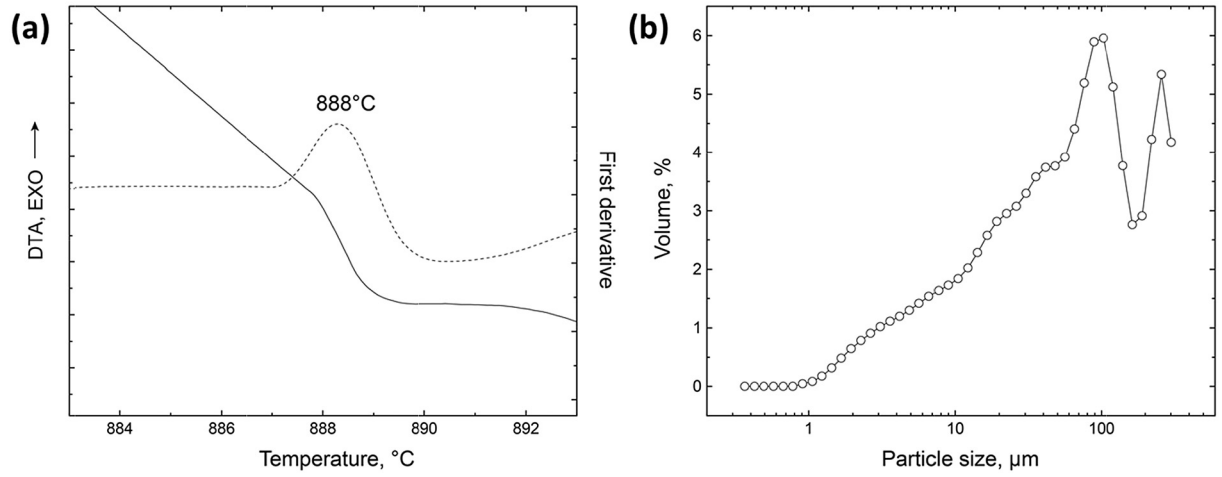

Fig. 1. DTA analysis (a) and particle size distribution of the porous silica powder (b).

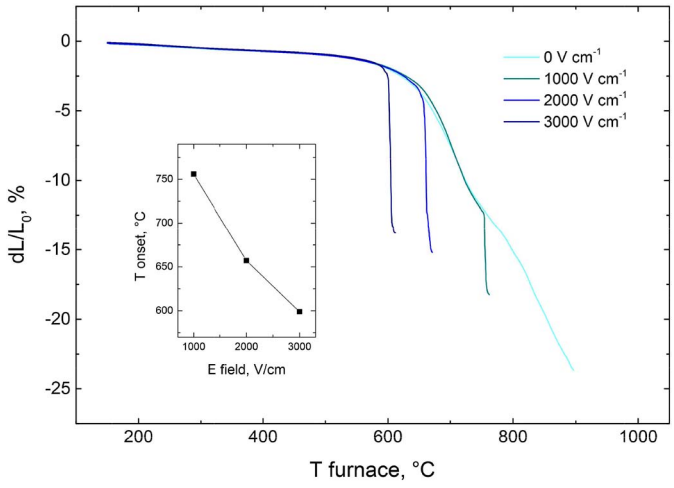

Fig. 2. Dilatometric plot recorded using different electric fields and current limit of 60 mA. The onset flash sintering temperature is reported in the inset.

field by itself (i.e., without current and power dissipation) does not interact with the viscous properties of the glass powder compact. Consequently, electric current and power dissipation are responsible for the observed phenomenon much more than the E-field.

The XRD patterns recorded on the anodic and cathodic surfaces of flash sintered samples are reported in Fig. 3. The spectra point out that, after the flash sintering process, both sample sides are still amorphous and no crystallization occurred.

On the basis of the collected results, we can point out that flash sintering can be successfully applied to materials typically characterized by viscous flow sintering, maintaining the initial amorphous network, the main densification phenomena being reproduced upon the flash regime. In addition, the flash event can be effectively reproduced, although the glass used in the present work is quite resistive, due to the limited sodium content (2.3 wt%). Nevertheless, we can also point out that the field/temperature here required for flash sintering are significantly higher than those needed for the Electric Field-Induced Softening (EFIS) reported in a previous work [19], the electric field used here being about one order of magnitude larger. Such differences are very likely associated to the higher glass electric resistivity. It can also be partially associated to the fact that EFIS experiments were carried out on bulk glasses, while here the electric field was applied to a powder compact, the presence of porosity clearly reducing the cross section available for current flow. A second fundamental difference is associated to the different chemical composition, alkali oxide load being 2.3 wt% in the present work and about 30–33 mol% in EFIS experiments [19] with obvious consequences in the electrical conductivity [27].

3.2. Electrical behavior of the samples during flash sintering

The electrical behavior of the samples during FS experiments is reported in Fig. 4. At low temperature, there is an almost linear relationship between log(J) and 1000/T, the current slowly increasing with temperature. Then, a strong deviation from the Arrhenius conductivity behavior, associated to the flash event, takes place. Such phenomenon has been always observed in flash sintering experiments; nevertheless, in the present work it shows some peculiar features. At first, it takes place when the specific power dissipation reaches 0.26–2.41 mW mm^{-3}, such values being significantly lower than those usually needed for triggering flash sintering in crystalline materials (typically in the range 10 to 50 mW mm^{-3} [28]). Then, the power dissipation at the flash onset increases with the applied field: values equal to 0.26, 0.76, 2.41 mW mm^{-3} were measured for the samples treated using 1000, 2000 and 3000 V cm^{-1}, respectively. Generally, power dissipation at the flash onset is almost independent on the applied field [28]. However, an accurate analysis of power dissipation plots reported in previous papers [1,14,28,29] allows to point out that the flash transition typically takes place at specific power dissipation slightly increasing with decreasing the applied field. Therefore, the behavior observed in the present work is remarkably different from that usually reported.

Finally, the deviation from the pre-flash behavior is substantially instantaneous here and it occurs in a time interval shorter than the acquisition period of the multimeter (1 s). It results in a sharp increase of power dissipation and electrical conductivity. Conversely, in a typical flash sintering experiment on crystalline material, the deviation from the Arrhenius behavior is more continuous and slower [1,28,29]. Fig. 5 points out that the assumption of a generalized and homogeneous thermal runaway from Joule heating cannot explain the electrical behavior measured in the present work. In fact, the sample temperature growth at the flash onset is not sufficient to justify the abrupt electrical resistivity drop. The plot in Fig. 5 shows the conductivity evolution as a function of the inverse of the sample temperature, as calculated from Eq. (3): as a matter of fact, at the flash onset the conductivity remarkably deviates from the pre-flash quasi-linear behavior.

In addition, during the flash sintering incubation (right portion of the plots in Fig. 4), the conductivity increases with the applied field. Therefore, E vs. J relation deviates from the Ohm's law, similarly to the results reported for flash sintering of resistive ceramics like α-alumina [15,21].

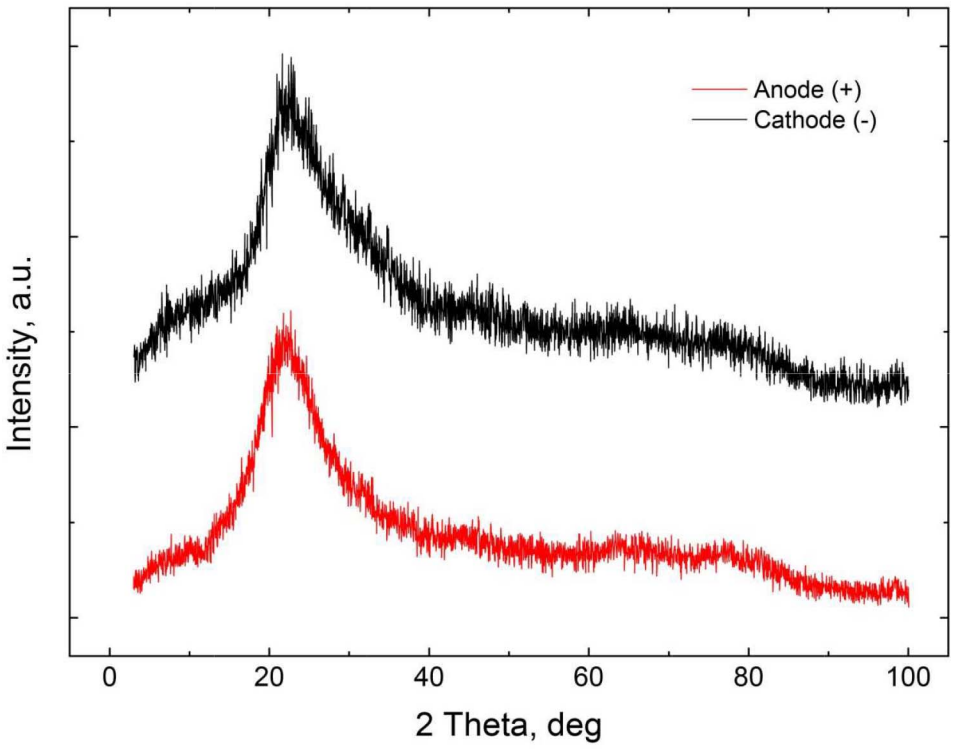

Fig. 3. XRD patterns obtained on the anode and cathode of the pellet sintered with 1000 V cm^{-1} and 60 mA.

Such features point out that the mechanisms which trigger flash sintering in this work are different from those previously reported, typically associated to a thermal runaway of Joule heating [12]. In particular, the almost instantaneous drop of the electrical resistivity suggests mechanisms based on spark, plasma formation or dielectric breakdown. It is worth to point out that if triggering mechanisms corresponds to interparticle plasma formation, similar results should be expected also in other materials under similar conditions of field/temperature. Actually, flash experiments using fields of 1000 V cm^{-1} or higher, were carried out in alumina [14,30] and glass-containing alumina [20], pointing out that the flash event is triggered at temperatures hundreds degrees above those experienced in the present work. This suggests that the instantaneous discharge observed at the flash event very likely is not caused by an interparticle plasma formation, but it probably involves the activation of dielectric breakdown of the glass. Indeed, the room temperature dielectric strength of oxide glasses is about three orders of magnitude larger than the fields applied in the present work [31]. However, this value strongly depends on temperature and it is dramatically reduced upon heating [32]. In addition, dielectric breakdown is stimulated at the glass/particle surface where the local field strength is enhanced by the presence of interfaces between media with different dielectric constants [15,33]. Such phenomenon is more effective in the initial stages of sintering when the pores are sharp and characterized by a low neck to particle radius ratio [33]. Finally, the field-enhanced conductivity during flash sintering incubation (Fig. 4(b)), resembles a pre-breakdown behavior, where the electrical conductivity increases with the applied field [34], this being similar to previous findings on α-alumina [15]. Therefore, it seems to represent a common feature in flash sintering experiments of highly resistive materials, where fields higher than 1000 V cm^{-1} are used.

3.3. Microstructure of the sintered samples

Although the flash event is almost instantaneous, the samples are

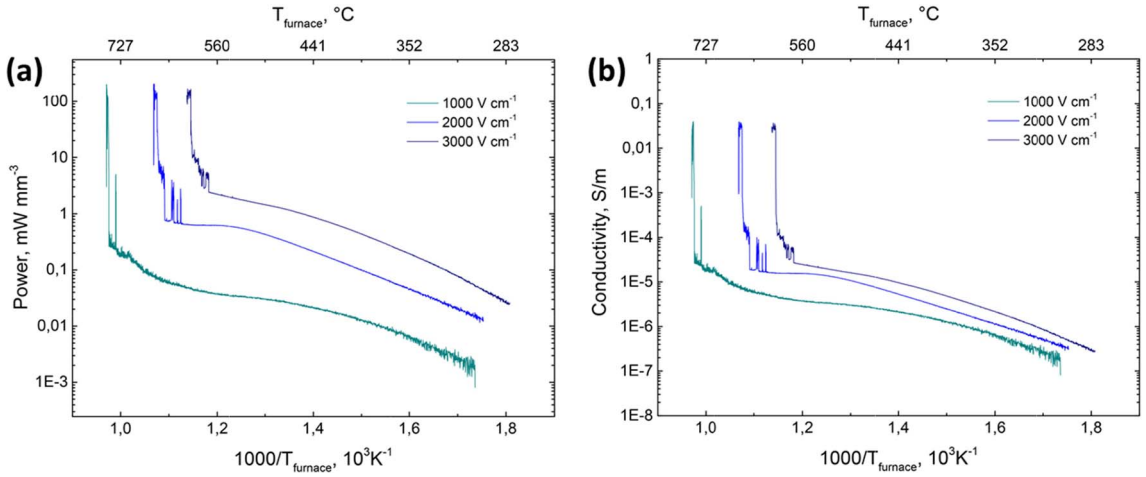

Fig. 4. Nominal specific power dissipation (a) and nominal electrical conductivity (b) as a function of 1000/T furnace.

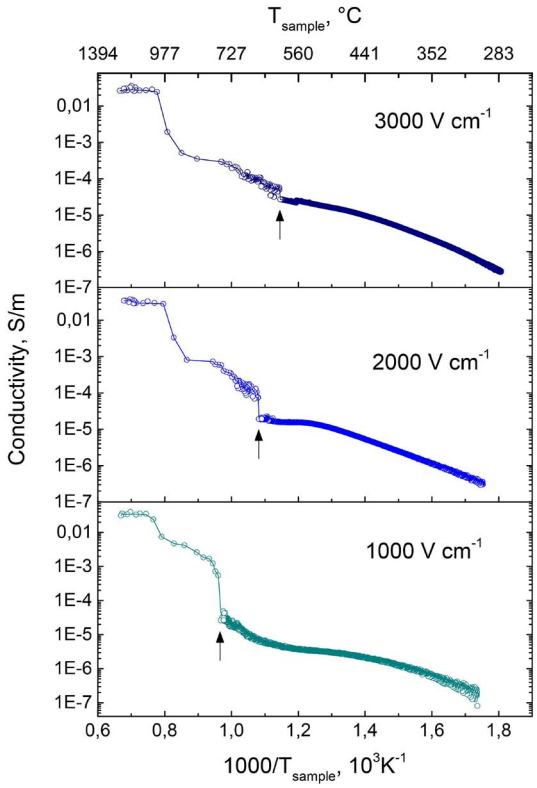

Fig. 5. Nominal electrical conductivity as a function sample temperature as calculated by Eq. (3). The black arrows point out where the material starts to deviate from the pre-flash behavior.

well densified and homogeneous (with the exception of the areas very closed to the electrodes). The microstructures of conventionally sintered (0 V cm^{-1}) and flash sintered (60 mA and 2000 V cm^{-1}) samples were compared in Fig. 6. It is substantially similar in the bulk with isolated, well distributed, spherical pores. For the flash sintered material a certain difference can be instead pointed out between the regions close to the electrodes (Fig. 6 (c,d)): while cathodic region appears to be dense, the anodic one is extremely porous, with cavities as large as 1 mm. Microstructural asymmetry associated to the DC field/current has already been reported in flash sintered crystalline ceramics. In such materials it is mainly associated to different grain coarsening kinetics [13,35,36]. It was attributed to electrolytic effects leading to a partial reduction of the oxidation state of metallic ions at the cathode or to field/current effect on the defect chemistry of the ceramic.

The origin of the microstructure differences found in the present work is not clear yet. It could be associated to an overheating of the anode, which leads to swelling phenomena due to the increased gas pressure in the closed pores. Anodic overheating during EFIS have been already pointed out by Yu et al. in a recent review on flash sintering [22]. However, it seems that the observed very sharp transition between normal/abnormal pores (Fig. 6) is unlikely to be due to temperature gradients.

Alternatively, the large pores formation at the anode can be associated to the anodic reaction:

$$O^{2-} \rightarrow \frac{1}{2}O_2 + 2e' \tag{4}$$

which leads to the formation of gaseous oxygen [37]. Such reaction is associated to electrolytic effects, which take place in alkali-containing glasses subjected to DC-electric current. The field breaks the Na—O bonds causing an electromigration of Na^+ ions toward the cathode, as shown in Fig. 7. The non-bridging oxygen atoms, which are no more saturated by sodium ions, are negatively charged and collapse, releasing O^{2-}. The oxygen ions move toward the anode where they are consumed by the anodic reaction given in Eq. (4) [37].

This hypothesis is supported by the EDS analysis reported in Fig. 8, which points out the formation of Na enriched region on the cathodic side of the specimen. Therefore, the glass is electrochemically active during the flash treatment. However, it is not clear whether such electrolytic phenomena (i.e., breakage of Na—O bonds) interact with the viscous properties, mass transport and densification.

The physical properties of the sintered specimens are summarized in Table 2. One can observe that in all the cases the final flash sintered specimen density is lower than that obtained via conventional sintering. However, by comparing the density results with SEM micrographs, we can state that such difference is mainly associated to the presence of

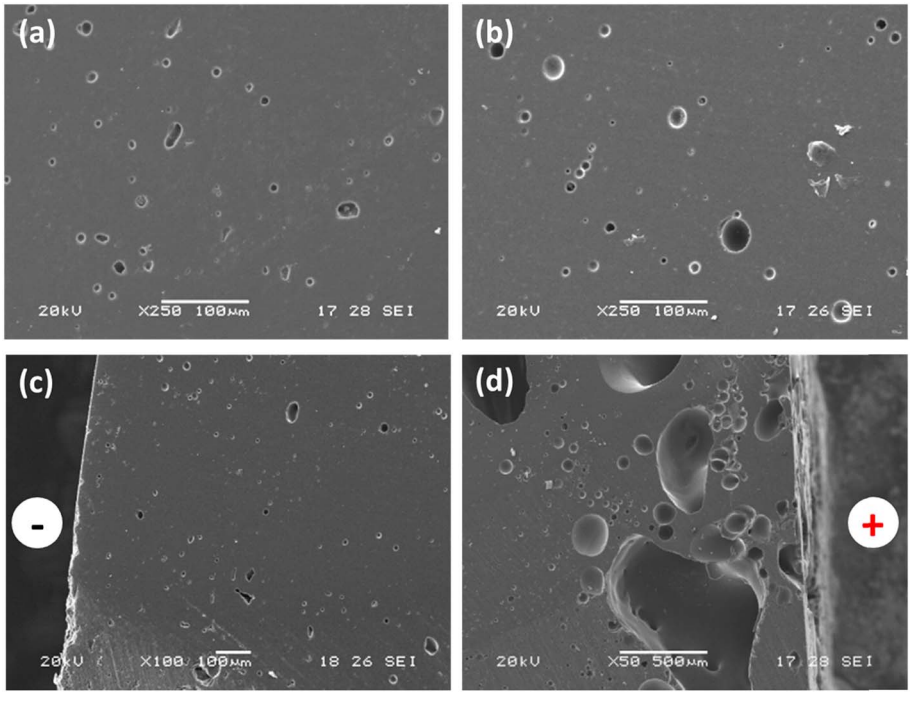

Fig. 6. SEM micrographs taken on a conventionally sintered sample (a) and on the central part of the sample flash sintered using 2000 V cm^{-1} and 60 mA (b). The microstructures of the cathodic (c) and anodic (d) area are reported for comparison.

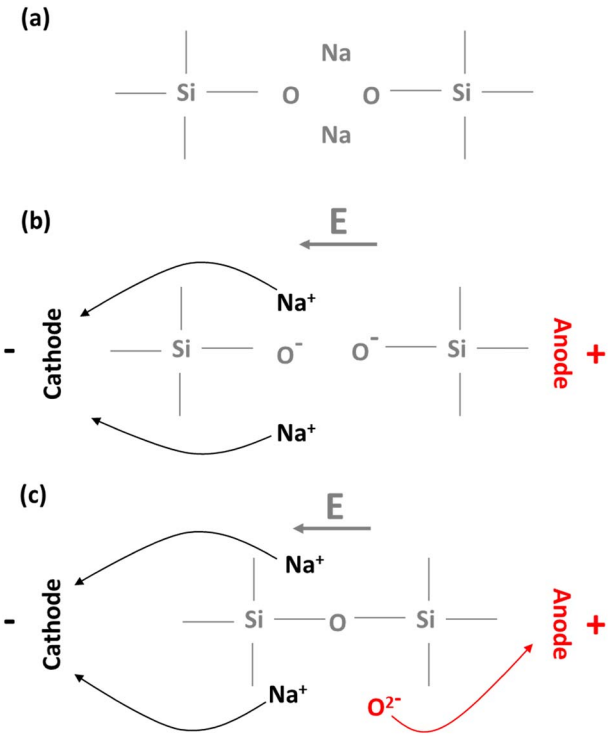

Fig. 7. Sodium ion migrations in a silicate glass under the effect of a DC field.

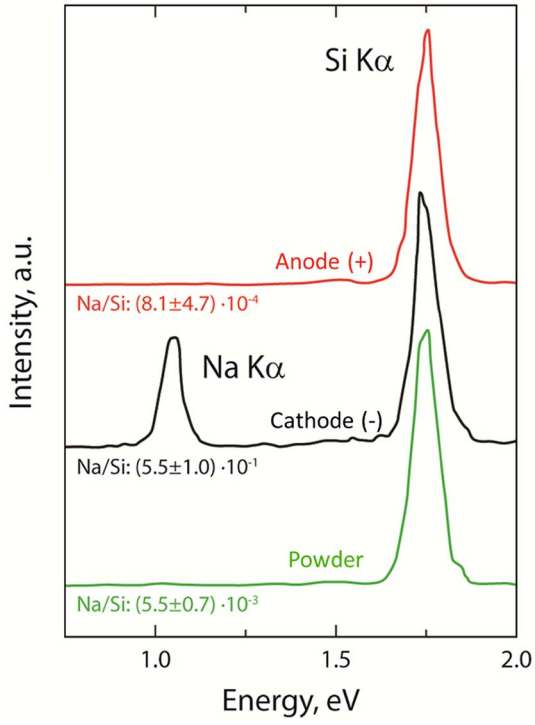

Fig. 8. EDS analysis of the anode and of the cathode of the sample flash sintered using 2000 V cm^{-1} and 60 mA, the analysis of the initial powder is reported for comparison. The "Na/Si" ratio reported in the figure represents the ratio between sodium and silicon EDS counts.

large pores in the anodic areas of the flash sintered samples. If the anodic zone is excluded, flash sintering provides a satisfactory densification of the material using 60 mA.

The effect of the current limit on densification was studied by reproducing flash sintering in isothermal experiments at 690 °C, the data being reported in Table 2. One can observe that at lower current limit (5–15 mA), the densification process is not completed and a large amount of open, interconnected porosity is still present after flash sintering. This is very likely associated to the lower temperature reached by the sample during the flash process (Table 2). Similarly, an increase of the current limit from 60 to 100 mA does not improve the densification. In the case of very high current, the sample temperature consistently increases and very likely causes over firing: the gas pressure within the closed pores grows at high temperature causing swelling and reduces the material density. Therefore, the results point out that the best densification is obtained using currents in the order of 60 mA, which corresponds to a current density of 2 mA mm^{-2}.

Table 2
Open porosity, bulk density and average sample temperature (estimated by Eq. (3)) in the steady stage of flash sintering (after the flash event) obtained in the different processes.

Nominal E (V cm^{-1})	Nominal I (mA)	Open porosity (± 0.1 vol%)	Bulk density (± 0.1 g cm^{-3})	T sample (°C)
Heating ramp 10 °C min^{-1}				
0	0	1.4	2.2	–
1000	60	4.5	2.1	1217 ± 38
2000	60	2.1	1.9	1210 ± 46
3000	60	4.9	1.9	1202 ± 34
Isotherm at 690 °C				
2000	5	28.6	1.6	833 ± 12
2000	15	17.0	1.8	972 ± 12
2000	60	6.2	1.9	1269 ± 30
2000	100	8.9	1.7	1398 ± 37

4. Conclusions

Porous silica glass powder (containing 2.3 wt% of Na_2O) pellets are densified by flash sintering using applied electric fields in the range 1000–3000 V cm^{-1} and a current limit of 2 mA mm^{-2}. The results point out the applicability of flash sintering to materials characterized by viscous flow sintering mechanisms. The microstructure of flash sintered specimens is comparable to that observed in conventionally sintered ones, although the DC-flash sintering process introduces microstructural asymmetry between anode and cathode (the former being more porous).

The conduction behavior in the pre-flash region does not follow the Ohm's low, the conductivity increasing with the applied field. In addition, the onset condition for flash sintering presents additional singular features, suggesting that the flash event is triggered by a dielectric breakdown.

Acknowledgement

One of the authors (MOP) would like to acknowledge Mag. Edison Rivera for the samples preparation and to the Agencia Nacional de Promoción Científica y Tecnológica de Argentina (ANPCyT) for partially funding this research through project PICT 2013-1403.

References

[1] M. Cologna, B. Rashkova, R. Raj, Flash sintering of nanograin zirconia in < 5 s at 850 °C, J. Am. Ceram. Soc. 93 (2010) 3556–3559.
[2] J.A. Downs, V.M. Sglavo, Electric field assisted sintering of cubic zirconia at 390 °C, J. Am. Ceram. Soc. 96 (2013) 1342–1344, http://dx.doi.org/10.1111/jace.12281.
[3] Y. Du, A.J. Stevenson, D. Vernat, M. Diaz, D. Marinha, Estimating Joule heating and ionic conductivity during flash sintering of 8YSZ, J. Eur. Ceram. Soc. 36 (2016) 749–759.
[4] X. Hao, Y. Liu, Z. Wang, J. Qiao, K. Sun, A novel sintering method to obtain fully dense gadolinia doped ceria by applying a direct current, J. Power Sources 210 (2012) 86–91, http://dx.doi.org/10.1016/j.jpowsour.2012.03.006.
[5] E. Zapata-Solvas, S. Bonilla, P.R. Wilshaw, R.I. Todd, Preliminary investigation of flash sintering of SiC, J. Eur. Ceram. Soc. 33 (2013) 2811–2816.
[6] C. Schmerbauch, J. Gonzalez-Julian, R. Röder, C. Ronning, O. Guillon, Flash

sintering of nanocrystalline zinc oxide and its influence on microstructure and defect formation, J. Am. Ceram. Soc. 97 (2014) 1728–1735.
[7] A. Gaur, V.M. Sglavo, Flash-sintering of MnCo2O4 and its relation to phase stability, J. Eur. Ceram. Soc. 34 (2014) 2391–2400.
[8] R. Muccillo, E.N.S. Muccillo, Electric field-assisted flash sintering of tin dioxide, J. Eur. Ceram. Soc. 34 (2014) 915–923.
[9] K.S. Naik, V.M. Sglavo, R. Raj, Field assisted sintering of ceramic constituted by alumina and yttria stabilized zirconia, J. Eur. Ceram. Soc. 34 (2014) 2435–2442.
[10] S. Grasso, T. Saunders, H. Porwal, B. Milsom, A. Tudball, M. Reece, I.W. Chen, Flash Spark Plasma Sintering (FSPS) of alfa and beta-SiC, J. Am. Ceram. Soc. 99 (2016) 1534–1543.
[11] S. Grasso, T. Saunders, H. Porwal, O. Cedillos-Barraza, D.D. Jayaseelan, W.E. Lee, M.J. Reece, Flash spark plasma sintering (FSPS) of pure ZrB2, J. Am. Ceram. Soc. 97 (2014) 2405–2408, http://dx.doi.org/10.1111/jace.13109.
[12] R.I. Todd, E. Zapata-Solvas, R.S. Bonilla, T. Sneddon, P.R. Wilshaw, Electrical characteristics of flash sintering: thermal runaway of Joule heating, J. Eur. Ceram. Soc. 35 (2015) 1865–1877.
[13] Y. Zhang, J. Il Jung, J. Luo, Thermal runaway, flash sintering and asymmetrical microstructural development of ZnO and ZnO-Bi2O3 under direct currents, Acta Mater. 94 (2015) 87–100.
[14] M. Biesuz, V.M. Sglavo, Flash sintering of alumina: effect of different operating conditions on densification, J. Eur. Ceram. Soc. 36 (2016) 2535–2542.
[15] M. Biesuz, P. Luchi, A. Quaranta, V.M. Sglavo, Theoretical and phenomenological analogies between flash sintering and dielectric breakdown in α-alumina, J. Appl. Phys. 120 (2016) 145107.
[16] K. Terauds, J.M. Lebrun, H.H. Lee, T.Y. Jeon, S.H. Lee, J.H. Je, R. Raj, Electroluminescence and the measurement of temperature during stage III of flash sintering experiments, J. Eur. Ceram. Soc. 35 (2015) 3195–3199.
[17] J.M. Lebrun, R. Raj, A first report of photoemission in experiments related to flash sintering, J. Am. Ceram. Soc. 97 (2014) 2427–2430.
[18] M. Biesuz, P. Luchi, A. Quaranta, A. Martucci, V.M. Sglavo, Photoemission during flash sintering: an interpretation based on thermal radiation, J. Eur. Ceram. Soc. 37 (2017) 3125–3130.
[19] C. McLaren, W. Heffner, R. Tessarollo, R. Raj, H. Jain, Electric field-induced softening of alkali silicate glasses, Appl. Phys. Lett. 107 (2015) 1–6.
[20] M. Biesuz, V.M. Sglavo, Liquid phase flash sintering in magnesia silicate glass-containing alumina, J. Eur. Ceram. Soc. 37 (2017) 705–713.
[21] M. Cologna, J.S.C. Francis, R. Raj, Field assisted and flash sintering of alumina and its relationship to conductivity and MgO-doping, J. Eur. Ceram. Soc. 31 (2011) 2827–2837.
[22] M. Yu, S. Grasso, R. Mckinnon, T. Saunders, M.J. Reece, Review of flash sintering: materials, mechanisms and modelling, Adv. Appl. Ceram. 116 (2017) 24–60.
[23] R. Chaim, Particle surface softening as universal behaviour during flash sintering of oxide nano-powders, Materials (Basel) 10 (2017).
[24] R. Chaim, Liquid film capillary mechanism for densification of ceramic powders during flash sintering, Materials (Basel). 9 (2016) 19–21.
[25] R. Chaim, G. Chevallier, A. Weibel, C. Estournès, Flash sintering of dielectric nanoparticles as a percolation phenomenon through a softened film, J. Appl. Phys. 121 (2017) 145103.
[26] I.J. Hewitt, A.A. Lacey, R.I. Todd, I.J. Hewitt, R.I. Todd, A mathematical model for flash sintering, Math. Model. Nat. Phenom. 10 (2015) 77–89.
[27] W. Martinsen, Selected Properties of Sodium Silicate Glasses and their Structural Significance, Iowa State University of Science and Technology, 1969, http://lib.dr.iastate.edu/cgi/viewcontent.cgi?article=5128&context=rtd.
[28] R. Raj, Analysis of the power density at the onset of flash sintering, J. Am. Ceram. Soc. 99 (2016) 3226–3232.
[29] M. Cologna, A.L.G. Prette, R. Raj, Flash-sintering of cubic yttria-stabilized zirconia at 750 °C for possible use in SOFC manufacturing, J. Am. Ceram. Soc. 94 (2011) 316–319.
[30] M. Biesuz, V.M. Sglavo, Field-assisted sintering of silicate glass-containing alumina, Ceram. Eng. Sci. Proc. 36 (2015) 75–81.
[31] L.I. Berger, Dielectric strength of insulating materials, in: William M. Haynes (Ed.), CRC Handb. Chem. Phys, 96th ed., CRC Press, 2016.
[32] A. von Hippel, R.J. Maurer, Electric breakdown of glasses and crystals as a function of temperature, Phys. Rev. 59 (1941) 820–823.
[33] T.B. Holland, U. Anselmi-Tamburini, D.V. Quach, T.B. Tran, A.K. Mukherjee, Local field strengths during early stage field assisted sintering (FAST) of dielectric materials, J. Eur. Ceram. Soc. 32 (2012) 3659–3666.
[34] J. Frenkel, On pre-breakdown phenomena in insulators and electronic semi-conductors, Phys. Rev. 54 (1938) 647–648.
[35] W. Qin, H. Majidi, J. Yun, K. van Benthem, Electrode effects on microstructure formation during FLASH sintering of yttrium-stabilized zirconia, J. Am. Ceram. Soc. 99 (2016) 2253–2259.
[36] H. Yoshida, P. Biswas, R. Johnson, M.K. Mohan, Flash-sintering of magnesium aluminate spinel (MgAl2O4) ceramics, J. Am. Ceram. Soc. 100 (2017) 554–562.
[37] A.K. Varshneya, Fundamentals of Inorganic Glasses, Academic Press, Inc., 1994.